Supplementary Information

Chirality Induced *Operando* Probing of Analyte-Surface Hybrid States in Heterogeneous Redox Processes

Nirman Chakraborty,[1] Subhajit Nandy,[2] Souvik Bhattacharjee,[3] Maximilian Pfeiffer,[1] Esmaeil Adabifiroozjaei,[4] Leopoldo Molina-Luna[4] and Christian Hess[1]*

[1]Eduard Zintl Institute of Inorganic and Physical Chemistry, Technical University of Darmstadt, 64287 Darmstadt, Germany

[2]Deutsches Elektronen-Synchrotron DESY, Notkestr. 85, 22607 Hamburg, Germany

[3]School of Physical Sciences, Indian Association for the Cultivation of Science, 2A & B Raja S. C. Mullick Road, Kolkata 700032, India

[4]Advanced Electron Microscopy Division, Department of Materials- and Geosciences, Technical University of Darmstadt, 64287 Darmstadt, Germany

[*]Corresponding author: christian.hess@tu-darmstadt.de

Contents

1. Synthesis, structure and heterojunction related electrical measurements

All precursors for synthesis were used in their procured chemical forms. For a typical synthesis, 1.3 mmol of $CuSO_4.5H_2O$ (Sigma Aldrich, 99%) was mixed with 0.91 mol of sodium citrate dihydrate (Sigma Aldrich, 99%) in DI water and stirred uniformly for two hours, followed by addition of 5.3 mmol NaOH (Roth, 99%) solution dropwise, till a pH of 9 was achieved. The whole solution was allowed to mix overnight and then transferred to a stainless-steel autoclave kept at 120°C for 48 hours. The precipitate obtained was cleaned thrice by centrifuging with ethanol and dried at 60°C overnight. The as-prepared samples were tested using ambient condition thermogravimetric analysis (TGA) for detecting the calcination temperature. TGA studies showed a complete loss of water and other inorganic contents from 400°C onwards. The samples were then calcined at 600°C for 6 hours, followed by sieving using a 56 µm mesh. For Au loading, 1.5 mmol tetrachlorogold(III) acid $HAuCl_4 \cdot 3H_2O$ (Carl Roth, 99.9% purity metal basis) was added to the Cu solution as an additional step. After digesting the samples in aqua regia, the Au content in each sample was measured by Inductively Coupled Plasma Optical Emission Spectrometry (ICP OES). The amount of Au determined for CuO, Au_CuO_X, Au_CuO_Y and Au_CuO_Z, were 0, 1.1, 1.7 and 2.5 wt% respectively. Additional Au incorporation led to the formation of secondary crystal phases in CuO and consequent lattice distortions, and were therefore excluded from the present study (see Figure S1).

The Au@CuO heterojunctions were characterised by estimating the Schottky barrier by using the Equation (1)

$$I_{sat}=AA^*T^2e^{-\phi/KT} \qquad \text{(S1)},$$

where I_{sat} is the saturation current, A is the diode contact area, A* is the Richardson constant (979.36 A cm^{-2} K^{-2} for CuO), ϕ is the barrier height and T is the applied temperature (corresponding to a certain voltage).

Based on the use of Equation (2),

$$\ln (I/T^2)=-\phi/KT + \ln (AA^*) \qquad \text{(S2)},$$

the ϕ values for CuO, Au_CuO_X, Au_CuO_Y and Au_CuO_Z were calculated to be 1.01 eV, 0.981 eV, 0.921 eV and 0.901 eV (see Figure S3). This indicates an increment of the electron affinity of CuO with increasing Au loading, compensated by charge transfer from Au to CuO.

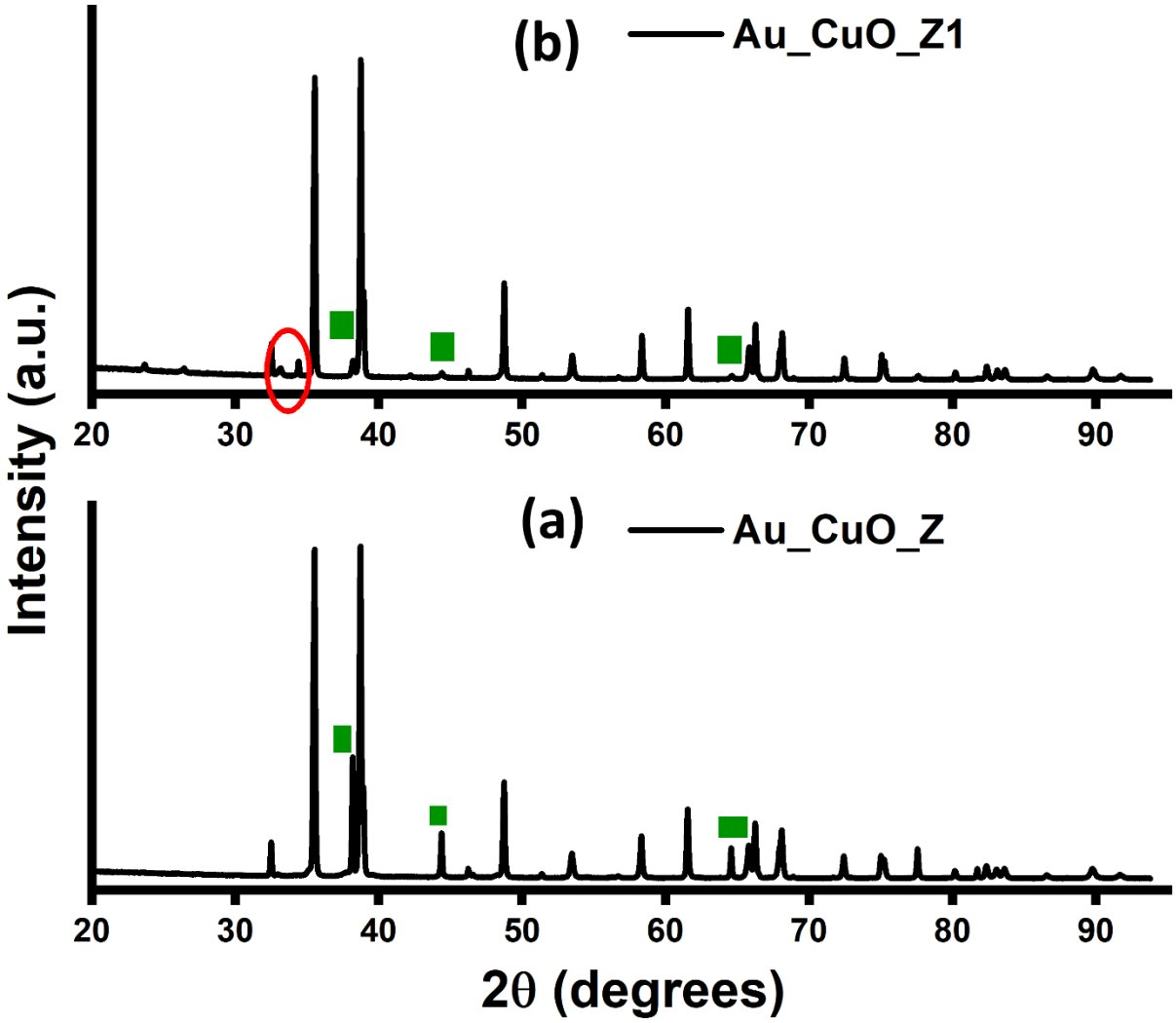

Figure S1. (a) Room temperature powder XRD pattern of Au_CuO_Z, with Au peaks marked using green symbols. (b) Composition Au_CuO_Z1 with greater Au content, is characterized by the formation of additional phases (marked in red).

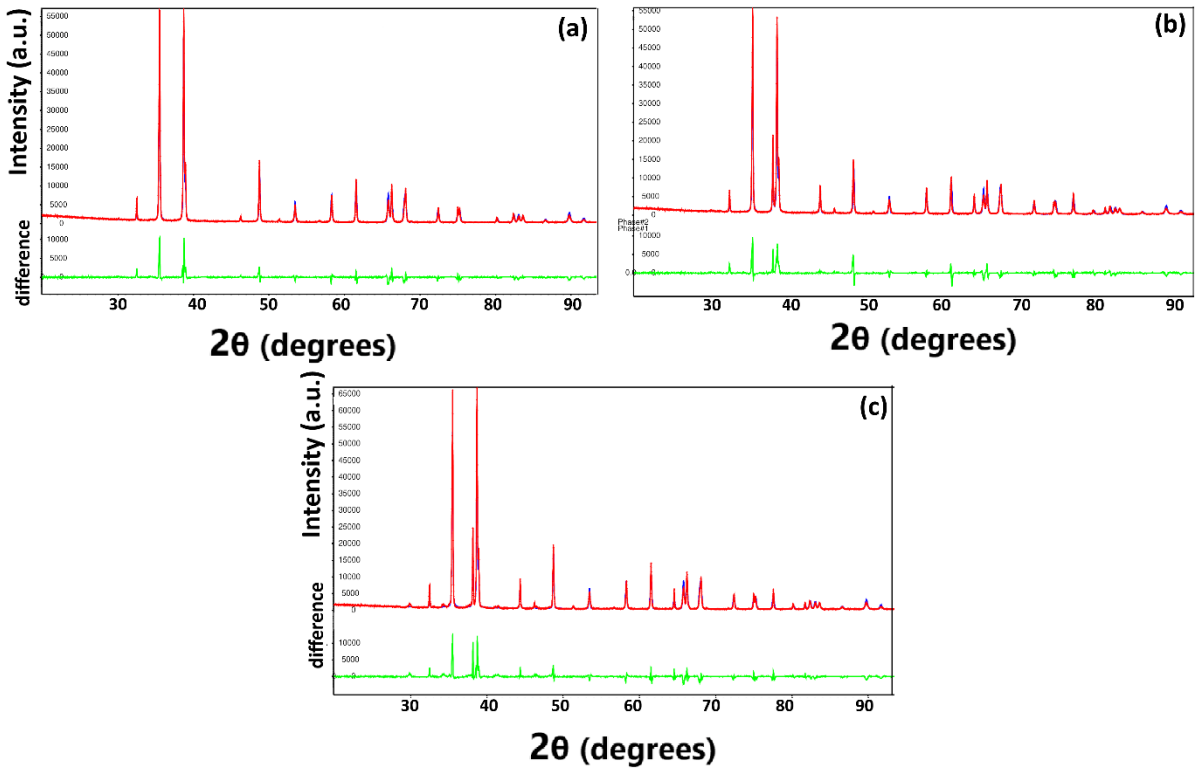

Figure S2. (a-c) X-ray diffractograms of CuO, Au_CuO_X, Au_CuO_Y, respectively, obtained from Rietveld refinement [R1]. Experimental points are shown in red, modelled points in blue and their difference in green.

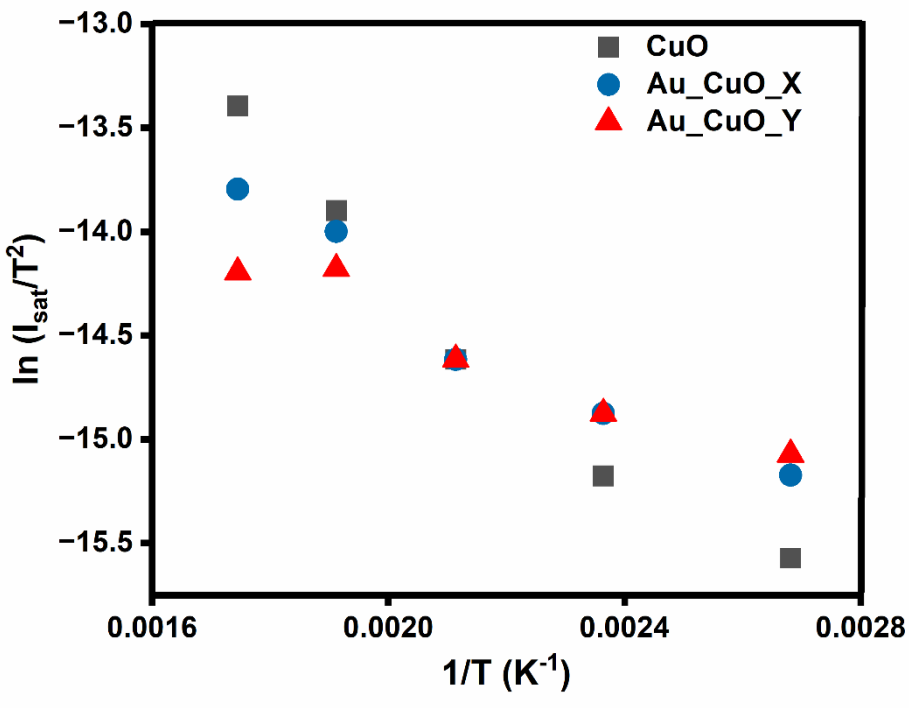

Figure S3. ln (I_{sat}/T^2) *vs*. 1/T plot to estimate the Schottky barrier for all samples, using Equations S1 and S2 mentioned in the above text.

Table S1. Details of the Rietveld refinement.

(a) CuO lattice (Rp, *w*Rp reliability & weighted reliability factors, respectively. GoF-Goodness of Fit)

Sample	$CuO_{0.991}$	Au_CuO (1.1%) $CuO_{0.989}$	Au_CuO (1.7%) $CuO_{0.986}$	Au_CuO (2.5%) $CuO_{0.984}$
Temperature	298 K	298 K	298 K	298 K
Space group	C2/c	C2/c	C2/c	C2/c
Lattice parameters				
a	4.68306(13)	4.6831(2)	4.68389(11),	4.6844(2)
b	3.42224(10)	3.42429(18)	3.42376(8),	3.42348(14)
c (Å)	5.12759(15)	5.1287(3)	5.12928(13)	5.1293(2)
α, β, γ (°)	90, 99.48, 90	90, 99.48, 90	90, 99.48, 90	90, 99.48, 90
V (Å^3)	81.055(4)	81.121(7)	81.132(3)	81.135(6)
R_p/*w*Rp	1.12/2.38	1.67/2.88	1.22/2.14	1.29/2.92
GoF	0.91	0.89	0.98	0.89
U_{iso} Cu	0.002	0.0024	0.0024	0.0024
O	0.01	0.01	0.01	0.01
Cu-O_{eq} (Å)	1.951(3)	1.956(4) (.25% expansion)	1.958(3) (.35% expansion)	1.959(2) (.41% expansion)
Cu-O_{polar} (Å)	1.9609(13)	1.9607(13)	1.9604(13)	1.9602(13)

(b) Au lattice

Sample	Au_CuO (1.1%) $CuO_{0.989}$	Au_CuO (1.7%) $CuO_{0.986}$	Au_CuO (2.5%) $CuO_{0.984}$
Space group	Fm3m	Fm3m	Fm3m
Lattice parameters			
a(Å)	4.07687(10)	4.07735(11)	4.07822(2)
α (°)	90	90	90
V (Å^3)	67.761(3)	67.785(3)	67.828(2)

R_p/wR_p GoF	1.41/1.88 0.87	1.12/2.04 0.92	1.11/2.72 0.85
U_{iso} Au	0.001	0.001	0.001

2. EXAFS fitting results

To further understand the local atomic environment near Cu atoms, a wavelet transformation using a Morlet wave function has been applied to the EXAFS signal. The Morlet wave function is written as [R2]

$$\psi(t) = \frac{1}{\sqrt{2\pi}\sigma}\,(e^{i\eta t} - e^{\frac{-\eta^2\sigma^2}{2}})e^{(-\frac{t^2}{2\sigma^2})} \quad \text{.....(S3)}$$

where η is the frequency of the sinusoidal wave and σ is the Gaussian wave full width at half maximum. Cu K-edge k^2 weighted χ(k) spectra are used for wavelet transform of CuO, Au_CuO_X and Au_CuO_Y, shown in the contour map (see Figure 1 in main text).

Table S2. Fitted parameters obtained from the Cu K-edge EXAFS signal. The fitted parameters are coordination number (N), bond distance (R in Å), inner potential shift (ΔE_0 in eV), and Debye-Waller factor (σ^2 in $Å^2$). The goodness of fit is represented by the R-factor.

Sample	Shell	N	R (Å)	ΔE_0 (eV)	σ^2 ($Å^2$)	R factor
CuO	Cu-O	4.0±0.1	1.941±0.003	-0.5	0.004±0.001	0.004
	Cu-O	2	2.881±0.007	7	0.002±0.001	
	Cu-Cu	10	2.987±0.007	-9.5	0.021±0.001	
Au_CuO_X	Cu-O	3.6±0.1	1.952±0.004	9	0.004±0.001	0.006
	Cu-O	2	2.863±0.010	5	0.002±0.001	
	Cu-Cu	10	3.043±0.020	8	0.028±0.003	
Au_CuO_Y	Cu-O	3.2±0.1	1.955±0.004	8.8	0.004±0.001	0.008
	Cu-O	2	2.875±0.011	7.0	0.002±0.001	
	Cu-Cu	10	3.090±0.025	8.0	0.030±0.005	

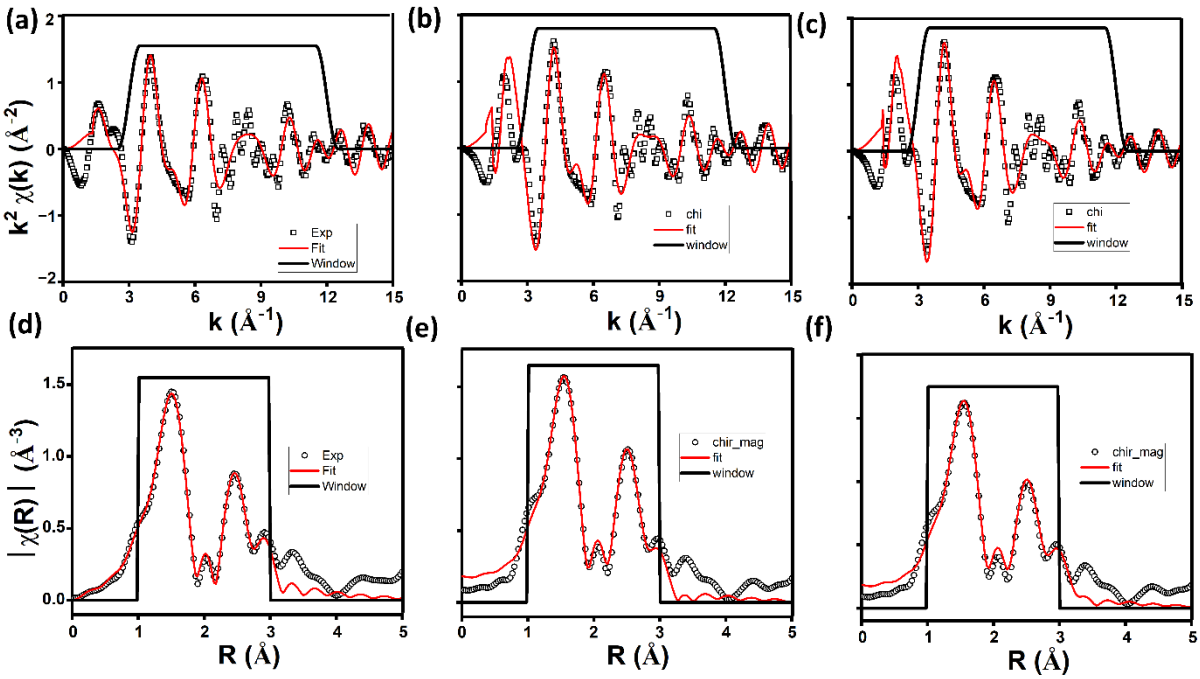

Figure S4. Cu K-edge (a-c) EXAFS signal of k^2 weighted $\chi(k)$ *vs.* k plots and (d-f) Fourier transform of the EXAFS signals in R-space of CuO, Au_CuO_X, Au_CuO_Y, respectively. Open symbols and solid lines represent experimental data and fitted curves respectively. The window shows the range of fitting.

3. TEM results

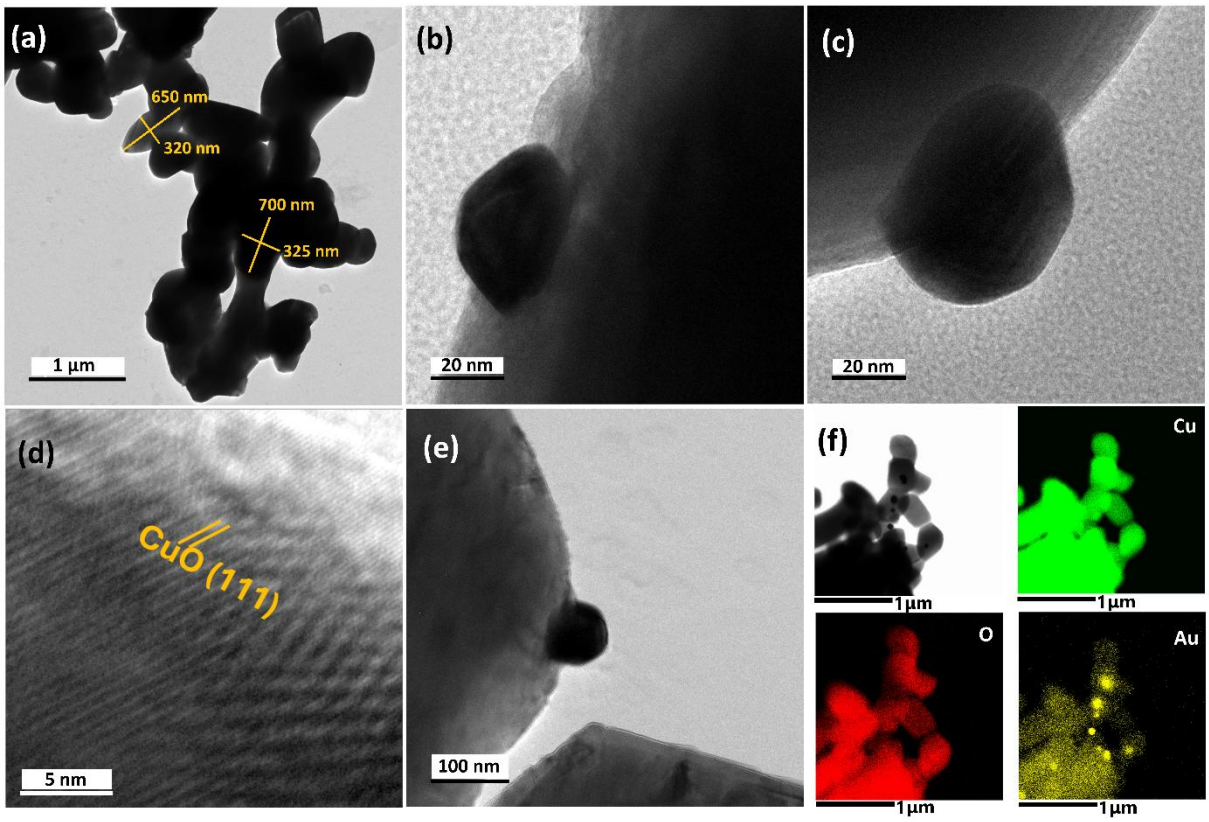

Figure S5. (a-c) Bright field TEM images of Au_CuO_X nanoparticles. The particle dimensions have been noted in (a) to visualize the size distribution. (d, e) HRTEM and Bright field TEM images of Au_CuO_Y nanoparticles, respectively. (f) EDX color mapping for Au_CuO_X nanoparticles, showing the Cu, O and Au distributions.

4. XPS results

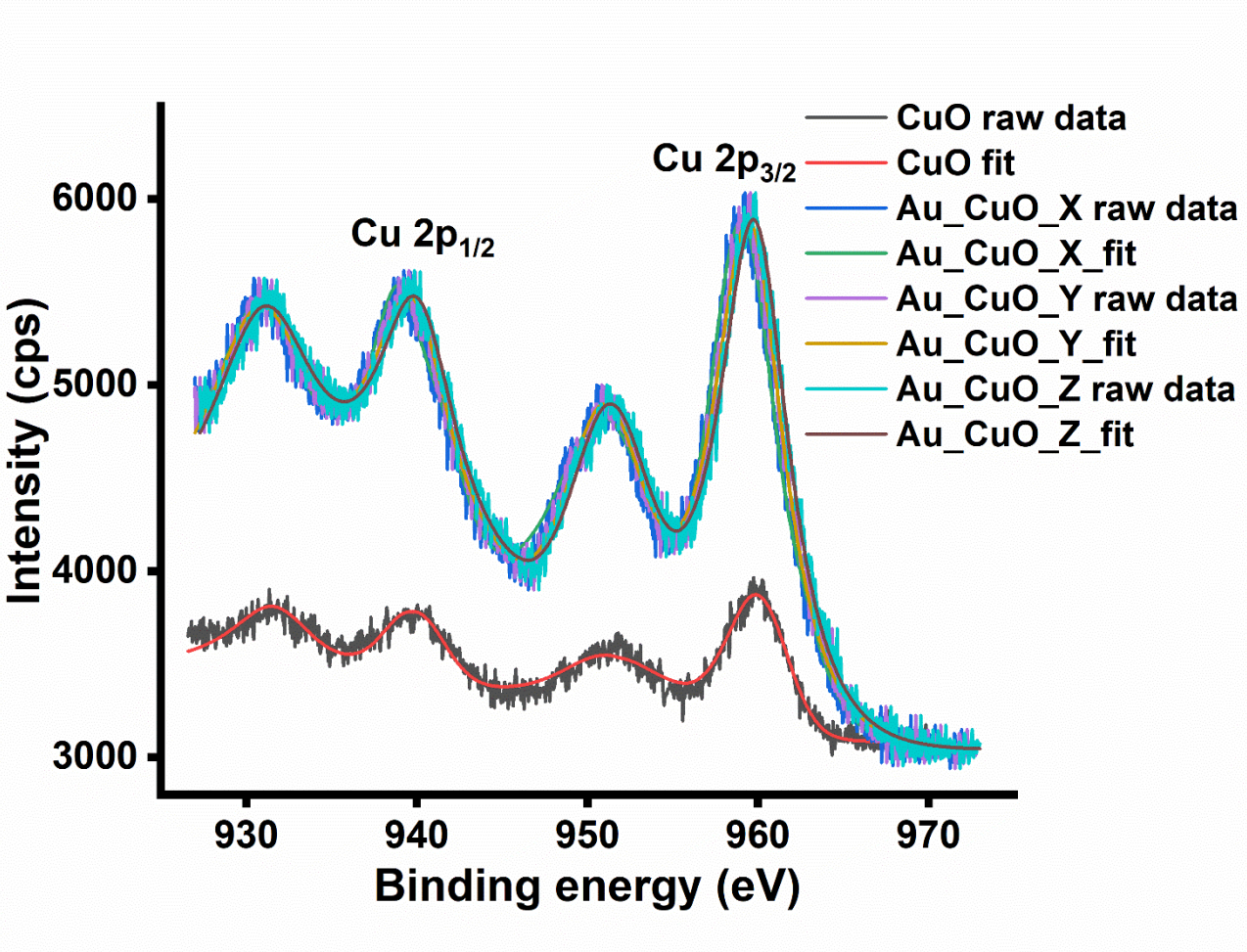

Figure S6. Cu 2p core level XP spectra for all samples, stacked together for comparison.

Table S3. XPS fitting details (SO-spin orbit, FWHM-full width half maxima, S1, S2-shake up peaks). O 1s* corresponds to surface -OH, as shown in Figure 2.

Sample (Au% from ICP)	**Peak**	**Binding energy (eV)**	**SO splitting (eV)**	**FWHM (eV)**	**Norm. peak areas**	**Ratio of areas**
CuO	Cu $2p_{3/2}$	933.5±0.05	19.9	4	100	1.9
	Cu $2p_{1/2}$	953.4±0.05		4	52.1	
	S1			6	38	
	S2			6	50	
	O 1s	531.3±0.05		2.8	151.7	
	O 1s*	531.9±0.05		2.8	4.13	
	C	284.8			52	
Au_CuO (1.1%)	Cu $2p_{3/2}$ Cu^{2+}/Cu^{+}	933.9/932.7±0.05	20/19.9	4	100/100	1.89/2.1
	Cu $2p_{1/2}$ Cu^{2+}/Cu^{+}	953.9/952.6±0.05		4	52.8/47.4	
	S1			6	60	
	S2			6	67	
	O 1s	531.5±0.05		2.8	297.66	
	O 1s*	532.1±0.05		2.8	15.2	
	Au $4f_{7/2}$	84.7±0.05	3.9	1.4	100	1.38
	Au $4f_{5/2}$	88.6±0.05		1.4	72	
	C	284.8			32.5	
Au_CuO (1.7%)	Cu $2p_{3/2}$ Cu^{2+}/Cu^{+}	934/932.9±0.05	20/19.8	4	100/100	1.94/2.07
	Cu $2p_{1/2}$ Cu^{2+}/Cu^{+}	954/952.7±0.05		4	51.5/48.2	

	S1			6	55	
	S2			6	62	
	O 1s	531.6±0.05		2.8	296.7	
	O 1s*	532.2±0.05		2.8	17.3	
	Au $4f_{7/2}$	84.8±0.05	3.9	1.4	100	1.47
	Au $4f_{5/2}$	88.7±0.05		1.4	68	
	C	284.8			24	
Au_CuO (2.5%)	Cu $2p_{3/2}$ Cu^{2+}/Cu^{+}	934.1/933±0.05	19.9/19.9	4	100/100	1.89/2.1
	Cu $2p_{1/2}$ Cu^{2+}/Cu^{+}	954/952.9±0.05		4	52.8/47.4	
	S1			6	60	
	S2			6	67	
	O 1s	531.8±0.05		2.8	296.5	
	O 1s*	532.3±0.05		2.8	19.4	
	Au $4f_{7/2}$	84.9±0.05	3.9	1.4	100	1.42
	Au $4f_{5/2}$	88.8±0.05		1.4	70	
	C	284.8			22	

5. Sensing measurements

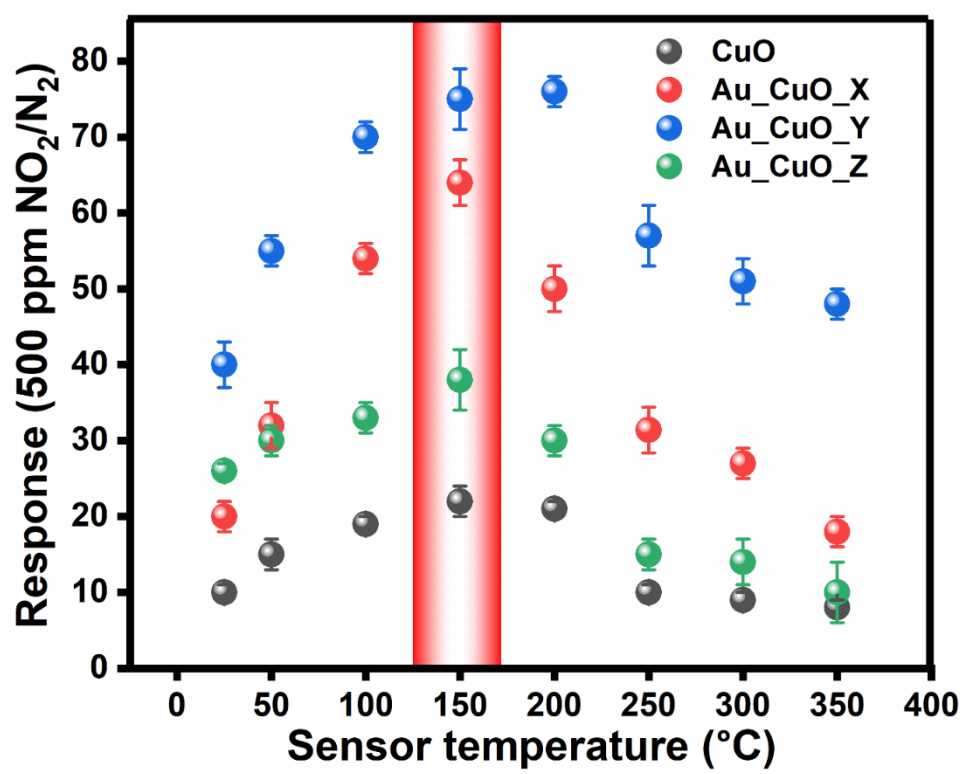

Figure S7. Sensing response *vs*. operational temperature for exposure to a feed of 500 ppm NO_2/N_2 for all samples. The region of optimum response has been highlighted in red. The error bars represent the experimental uncertainty for response values.

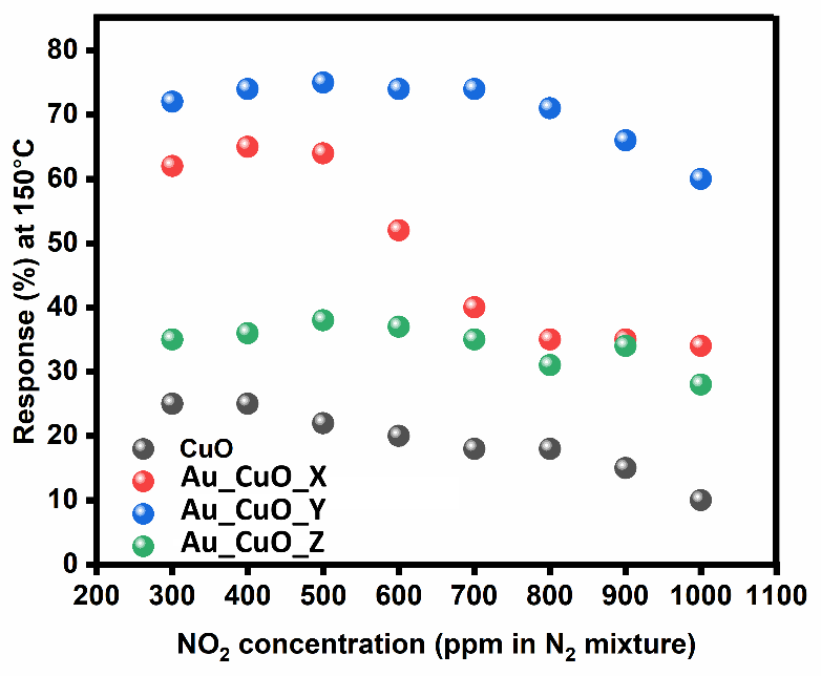

Figure S8. Sensing response *vs*. NO_2 concentration at 150°C operational temperature.

6. *Operando* UV-Vis measurements

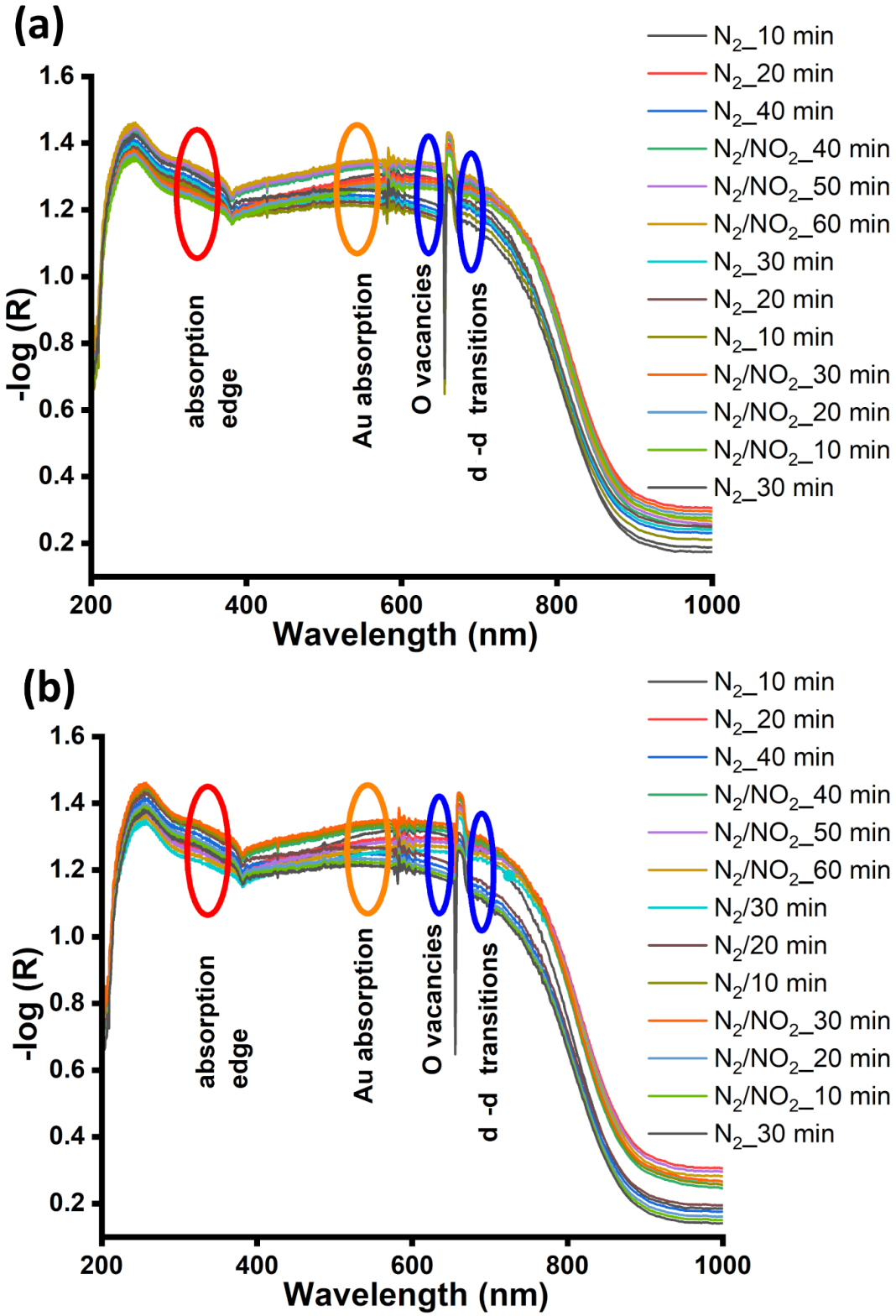

Figure S9. *Operando* UV-Vis spectra of the Au_CuO_Y sample at (a) 100°C and (b) 200°C operational temperature.

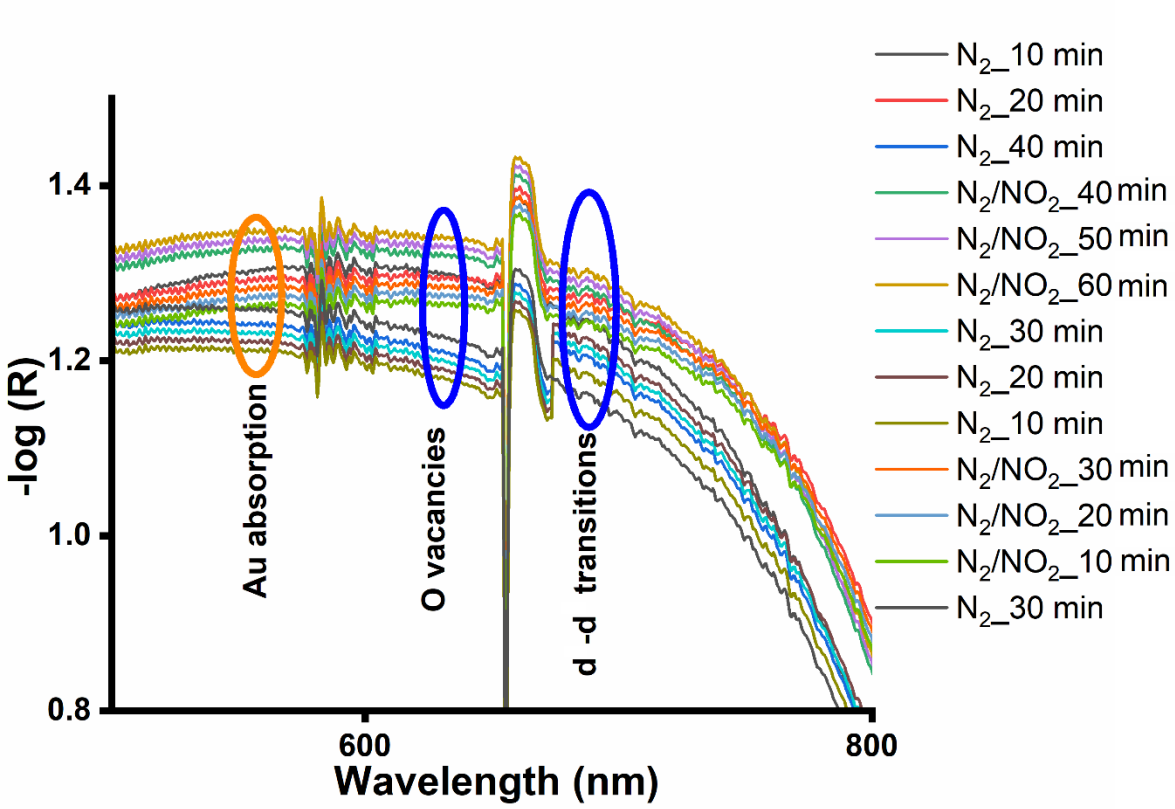

Figure S10. Enlarged UV-Vis *operando* spectra for Au_CuO_Y at 100°C highlighting the sequentially collected spectra and their variation. This graph represents an enlarged view of Figure 3(a) in the main text.

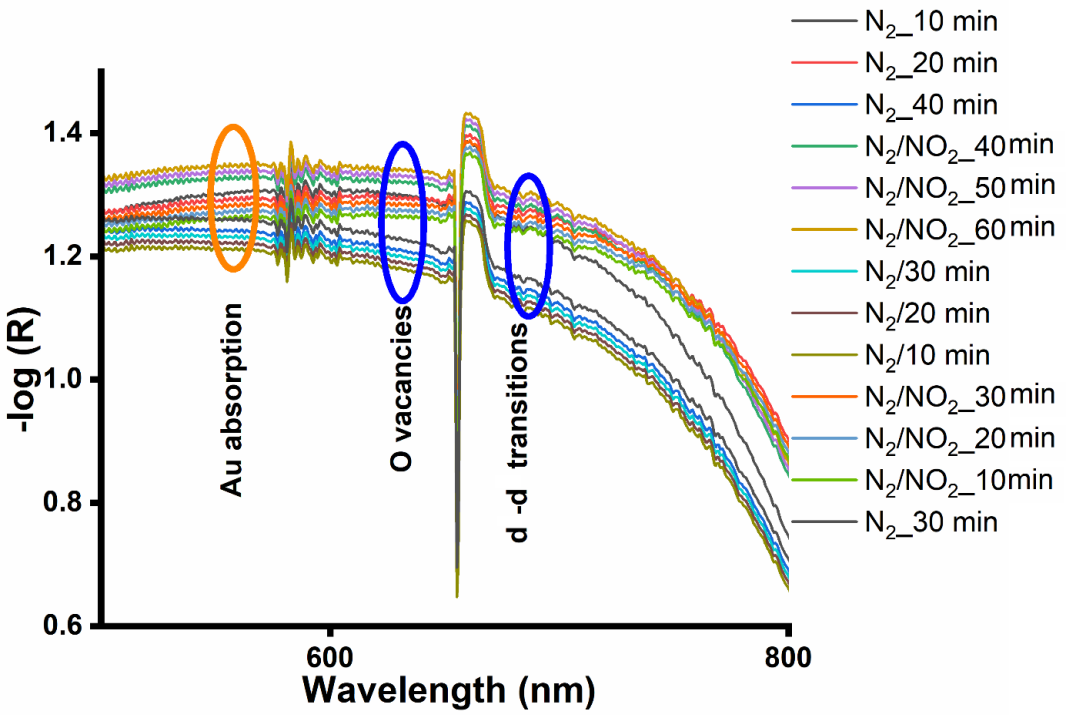

Figure S11. Enlarged UV-Vis *operando* spectra for Au_CuO_Y at 150°C, highlighting the sequentially collected spectra and their variation. A compact graph corresponding to this has been presented in Figure 3(a) in the main text.

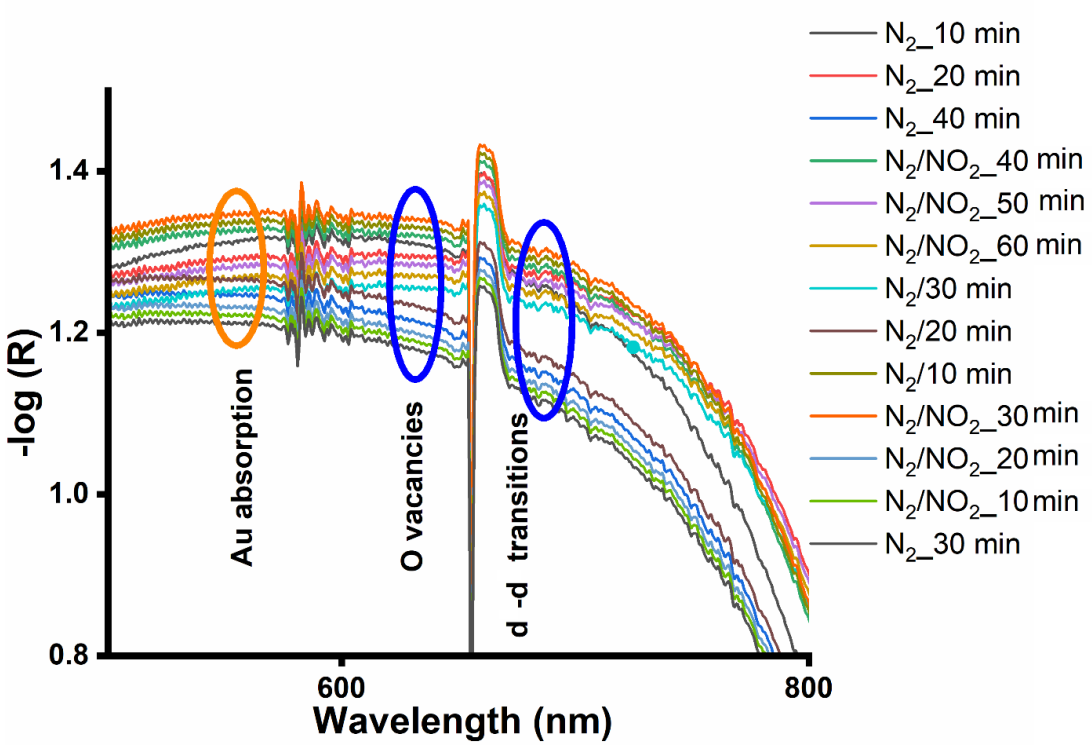

Figure S12. Enlarged UV-Vis *operando* spectra for Au_CuO_Y at 200°C (From figure S9(b)), highlighting the sequentially collected spectra and their variation.

7. *Operando* Raman measurements

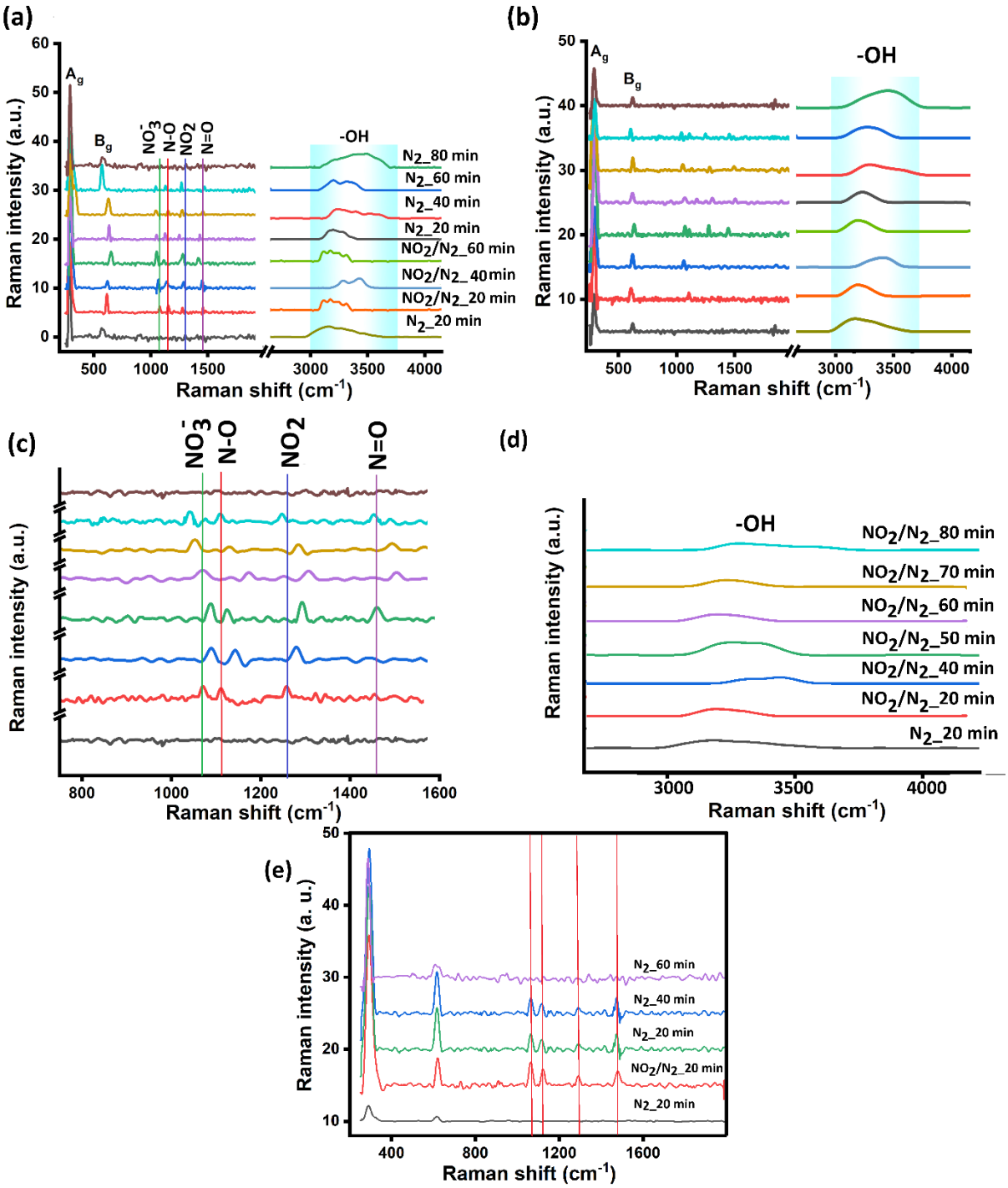

Figure S13. *Operando* Raman spectra of (a) Au_CuO_X and (b) Au_CuO_Z at 150°C. The experimental sequence in (b) is same as (a). (c) Enlarged view of (b) highlighting the NO_2-related vibrational modes. (d) Spectra of the -OH region of Au_CuO_Y at 150°C, with additional spectra collected after 50, 70 and 80 minutes. (e) Control experiment with

Au_CuO_Y showing effects of continued N_2 exposure after 20 minutes of 500 ppm NO_2/N_2 exposure. The NO_2 signals show no shift under identical environment, till they disappear.

Operando Raman spectra recorded after 40 minutes of exposure to NO_2/N_2 or N_2 (see in Figures 4(a) and S13(a)) reveal differences to those recorded before and after (e.g. 20 minutes or 60 minutes). Further analysis based on spectra recorded after 70 and 80 minutes reveal an overall similar behavior as that observed after 60 minutes (see Figure S13(d)), indicating that the intermediate spectra arise from an unsteady NO_2-OH reaction post the initial feed, which stabilizes eventually. This is represented by additional spectra collected after 50 minutes (see Figure S13(d)).

8. FTIR results

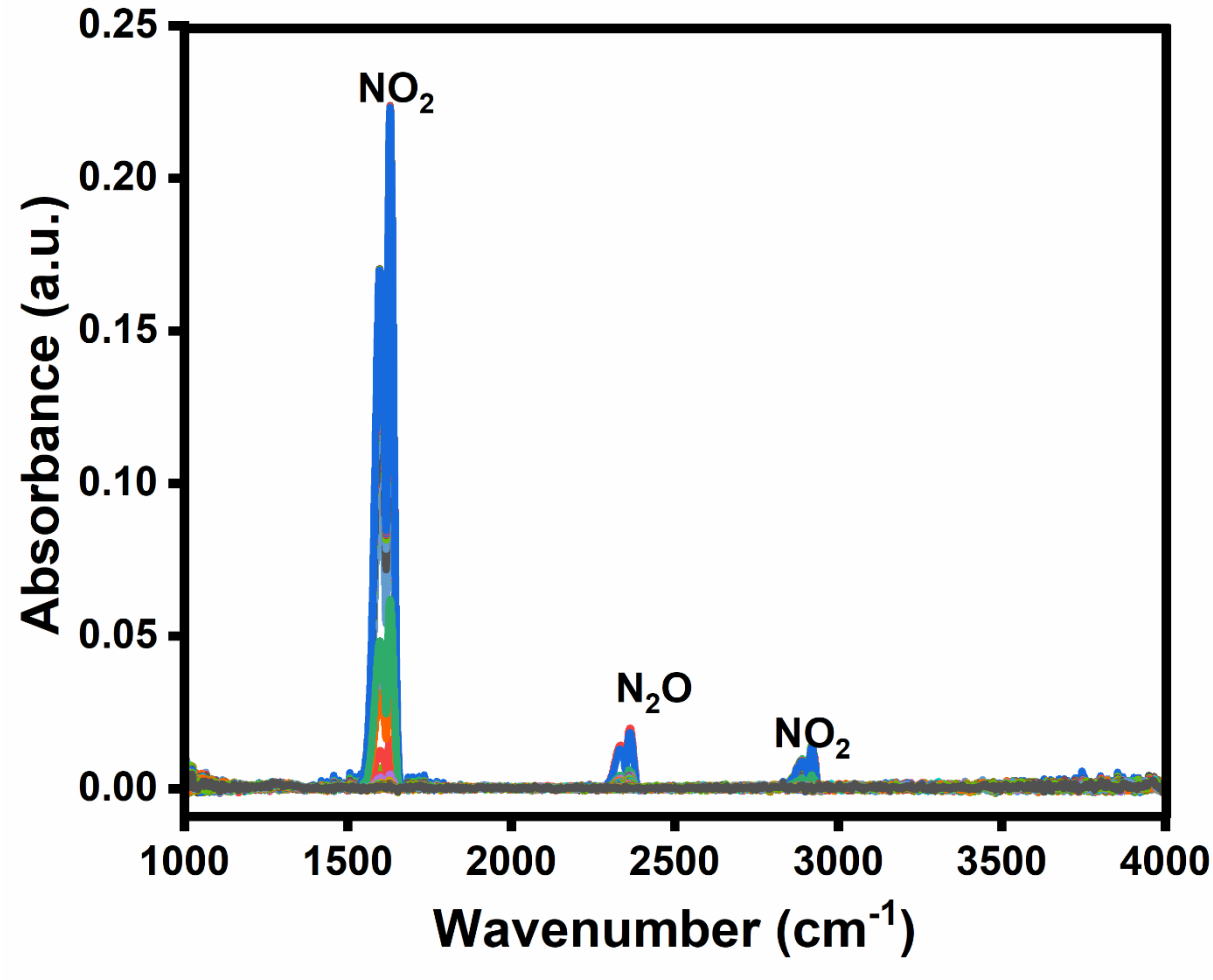

Figure S14. Gas phase composition during *operando* experiments at 150°C for bare CuO.

9. Stark effect measurements and analyses

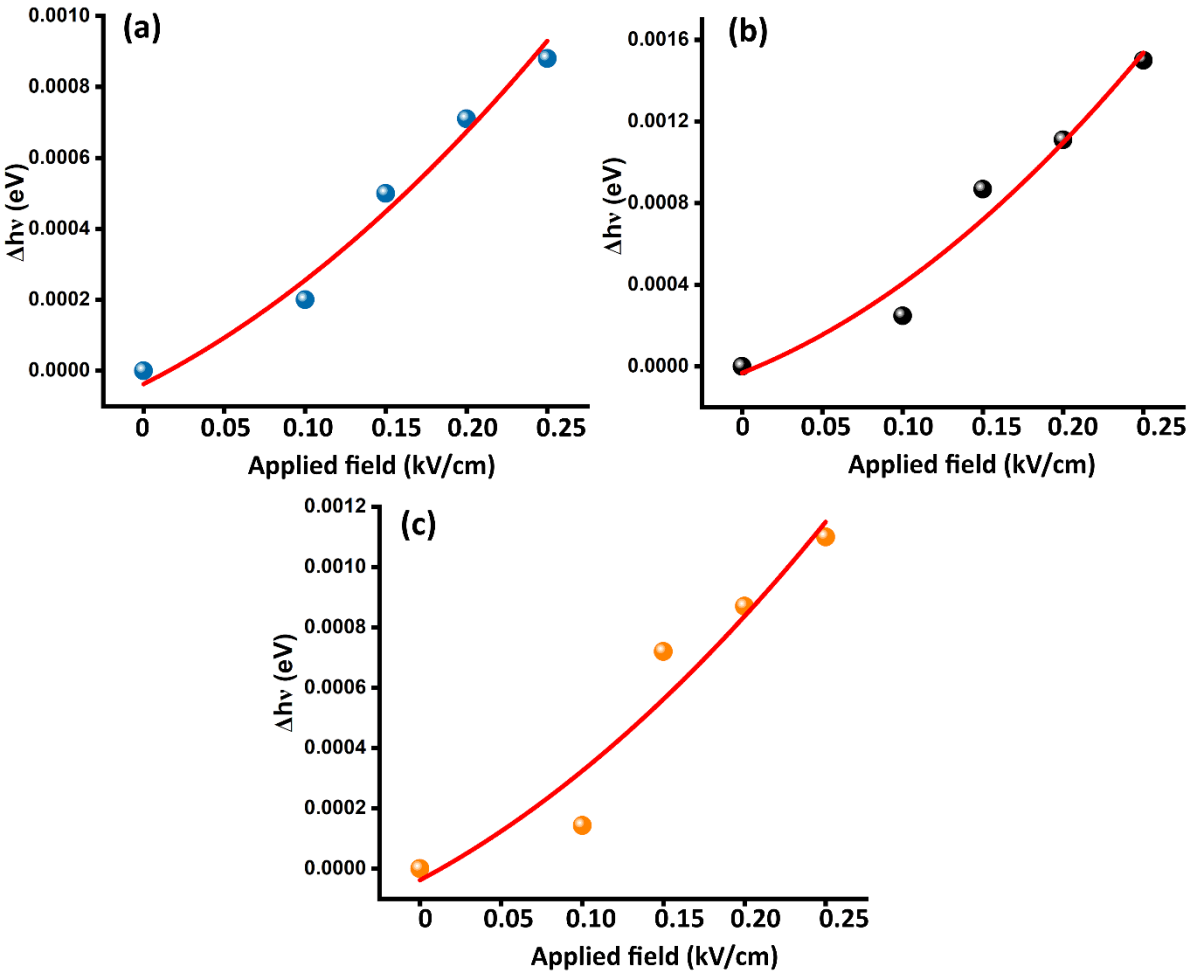

Figure S15. Non-linear curve fitting $y = A + B_1x^1 + B_2x^2$ of splitting energy *vs*. applied field for samples (a) Au_CuO_X, (b) Au_CuO_Y and (c) Au_CuO_Z, respectively.

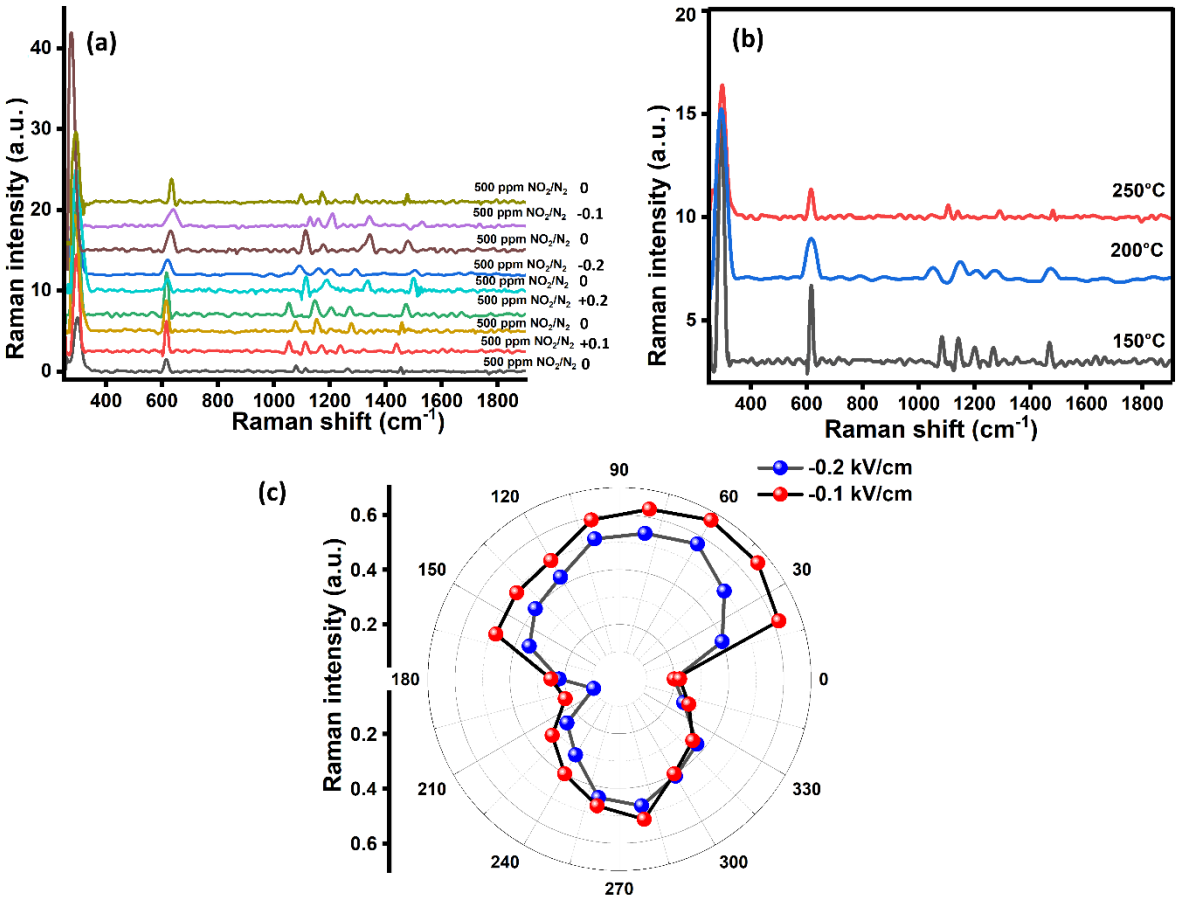

Figure S16. (a) Field on/off (at 150°C), with applied electric field in units of kV/cm. (b) temperature dependent experiments at applied external field of +0.1 kV/cm for the Au_CuO_Y sample. (c) Linearly polarized Raman analysis of external field applied-split peak in Au_CuO_Y sample, for two cases of -0.1 kV/cm and -0.2 kV/cm.

10. DFT results

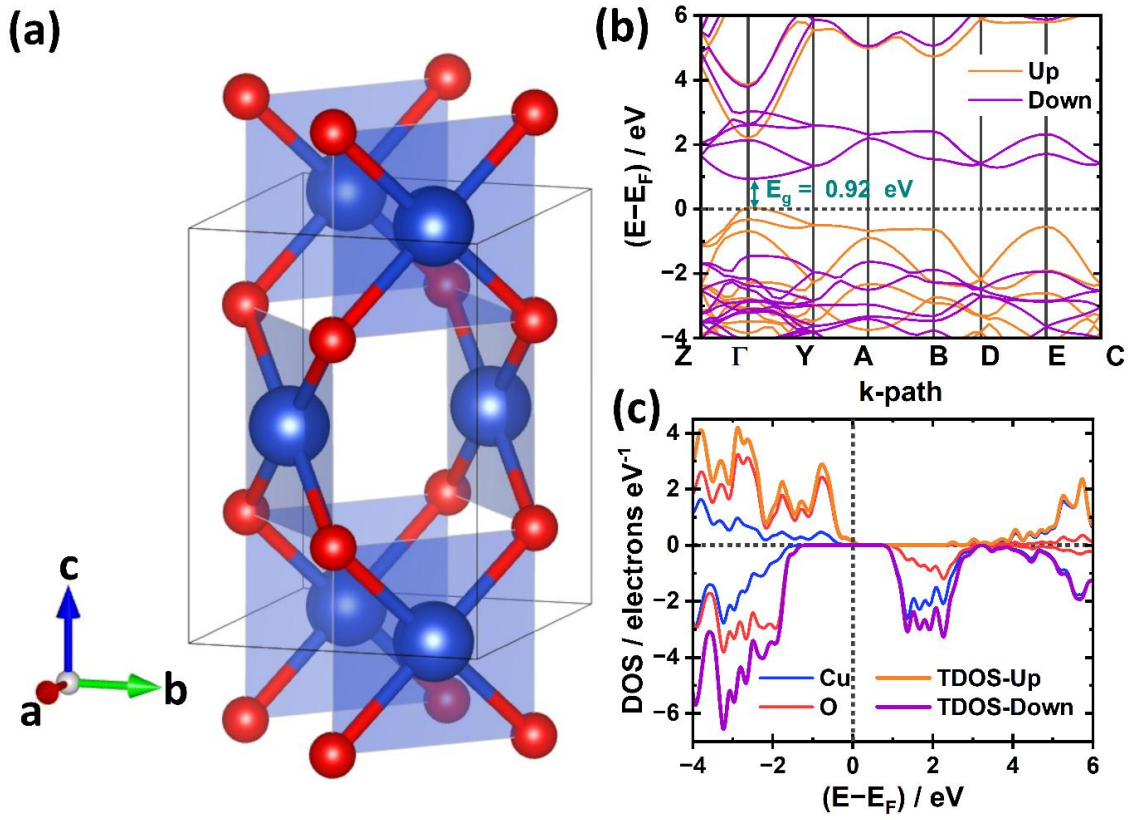

Figure S17. (a) Crystal structure of bulk CuO (blue spheres: Cu, red spheres: O). (b) Spin polarized band structure of bulk CuO. (c) Spin polarized DOS of bulk CuO.

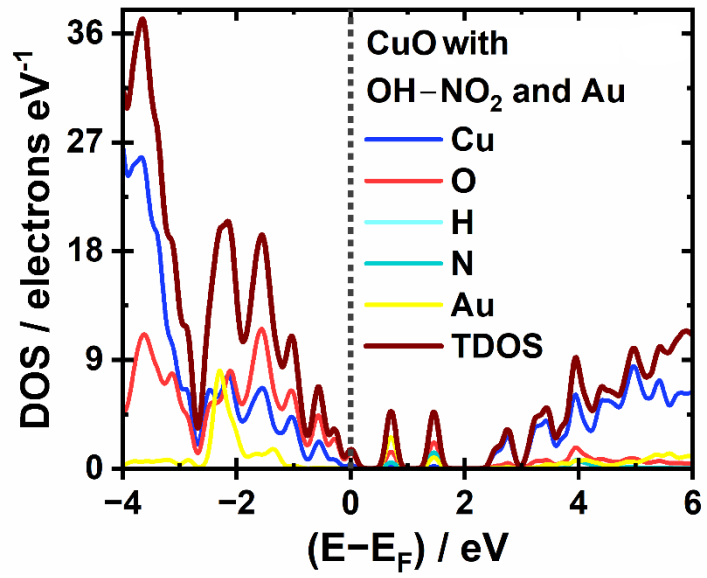

Figure S18. Majority spin DOS of Au@CuO with NO_2-OH surface reactions.

References

[R1] Rietveld, M. H. A Profile Refinement Method for Nuclear and Magnetic Structures. *J. Appl. Crystallogr.* **1969**, *2*, 65– 71.

[R2] Funke, H.; Scheinost, A. C.; Chukalina, M. Wavelet analysis of extended X-ray absorption fine structure data. *Phys. Rev. B* **2005**, *71*, 094110.